Formation of Native Disulfide Bonds in Endothelin-1. Structural Evidence for the Involvement of a Highly Specific Salt Bridge between the Prosequence and the Endothelin-1 Sequence†

André Aumelas,*,‡ Shigeru Kubo,§ Naoyoshi Chino,§ Laurent Chiche,‡ Eric Forest,|| Christian Roumestand,‡ and Yuji Kobayashi⊥

Faculté de Pharmacie, Centre de Biochimie Structurale, CNRS UMR C9955, INSERM U414, 34060 Montpellier Cedex 2, France, Peptide Institute, Inc., 4-1-2 Ina, Minoh, Osaka 562, Japan, Institut de Biologie Structurale, 41 avenue des Martyrs, 38027 Grenoble Cedex 1, France, and Institute for Protein Research and Faculty of Pharmaceutical Sciences, Osaka University, Suita, Osaka 565, Japan

Received September 25, 1997; Revised Manuscript Received December 16, 1997

ABSTRACT: The [Lys-Arg]-endothelin-1 analogue (KR-ET-1) yields almost selectively the native disulfide pattern (96%), in contrast to endothelin-1 (ET-1) that gives at least 25% of the non-native disulfide pattern. We have previously shown that the carboxylate-state structure of KR-ET-1 is more constrained and stabilized by a salt bridge between Arg(−1) and the Asp8 or Glu10 side chain [Aumelas et al. (1995) *Biochemistry 34*, 4546−4561]. To identify this salt bridge and its potential involvement in the disulfide bond formation, [E10Q], [D18N], and [D8N] carboxamide analogues were studied, which led to the unambiguous identification of the Arg(−1)−Asp8 salt bridge. Furthermore, while [E10Q] and [D18N] analogues gave a high yield of the native isomer (≥90%), the [D8N] analogue afforded a ratio of the two isomers close to that observed for ET-1 (68%) [Kubo et al. (1997) *Lett. Pept. Sci. 4*, 185−192]. Assuming that the formation of disulfide bonds occurs in a thermodynamically controlled step, we have hypothesized that the Arg(−1)−Asp8 salt bridge and concomitant interactions could be responsible for the increase in yield of the native isomer of KR-ET-1. In the present work, we describe the structural studies of the carboxamide analogues and of the minor non-native KR-ET-1 isomer. On the basis of ^{1}H NMR and CD spectra as a function of pH, [E10Q] and [D18N] analogues display a conformational change similar to that of the parent peptide, whereas the structure of the [D8N] analogue is unchanged. For the non-native isomer, we measured a lower helical content than for the native isomer and observed a marked difference in the orientation of the KRCSC backbone. In addition, no salt bridge was experimentally observed. Altogether, these results allow us to hypothesize that the salt bridge between two highly conserved residues, one belonging to the prosequence [Arg(−1)] and the other to the mature sequence [Asp8], is involved in the formation of the native disulfide isomer of ET-1. The involvement of the prosequence in the formation of the native disulfide isomer strongly suggests that, in the maturation pathway of ET-1, cleavage of the Arg52−Cys53 amide bond occurs after native disulfide bond formation.

While oxidation of the endothelin-1 peptide (ET-1) gives 25% of the non-native disulfide pattern (C1−C11 and C3−C15), the 23-residue peptide [Lys(−2)-Arg(−1)]-ET-1 (KR-ET-1),[1] containing the basic dipeptide Lys-Arg of the prosequence, yields almost selectively the native disulfide pattern (C1−C15 and C3−C11) (Figure 1). To understand how the Lys-Arg dipeptide from the prosequence is involved in the increase in native disulfide bond formation, the solution structure of KR-ET-1 was determined in a previous study based on CD and ^{1}H NMR experiments. Contrary to ET-1, the KR-ET-1 structure was found to depend on the ionization state of the carboxyl groups (*1*). In the carboxylic acid state, NMR-derived constraints yielded a solution structure characterized by the cystine-stabilized helical motif and by an unstructured C-terminal part as reported for ET-1 itself (*2*−*6*). In contrast, in the carboxylate state, the KR-ET-1 structure is characterized by a salt bridge involving the Arg-

† A.A. would like to thank the Japan Society for the Promotion of Science for financial support (Grant 103030).

* To whom correspondence should be addressed.
‡ Centre de Biochimie Structurale.
§ Peptide Institute, Inc.
|| Institut de Biologie Structurale.
⊥ Institute for Protein Research and Faculty of Pharmaceutical Sciences.

[1] Abbreviations: CD, circular dichroism; 1D and 2D, one- and two-dimensional; TSP-d_4, sodium 2,2,3,3-tetradeuterio-3-(trimethylsilyl)-propionate; DG, distance geometry; DBF-COSY, 2D double-band-filtered correlation spectroscopy; DQF-COSY, 2D double-quantum-filtered correlation spectroscopy; ESIMS, electrospray ionization mass spectroscopy; ET, endothelin; GSH and GSSG, reduced and oxidized glutathione; MD, molecular dynamics; NMR, nuclear magnetic resonance; NOE, nuclear Overhauser effect; NOESY, 2D nuclear Overhauser effect spectroscopy; RMSD, root-mean-square deviation; ROESY, rotating frame Overhauser effect spectroscopy; RP-HPLC, reverse-phase high-performance liquid chromatography; SA, simulated annealing; TOCSY, total correlation spectroscopy; TPPI, time proportional phase incrementation; KR-ET-1, [Lys(−2)-Arg(−1)]-endothelin-1; [D8N], [Asp8→Asn8]-KR-ET-1; [E10Q], [Glu10→Gln10]-KR-ET-1; [D18N], [Asp18→Asn18]-KR-ET-1.

S0006-2960(97)02376-3 CCC: $15.00
Published on Web 03/21/1998

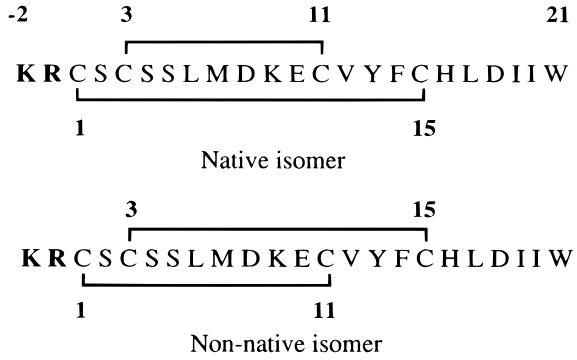

FIGURE 1: KR-ET-1 sequence and disulfide patterns of the native and non-native isomers. The Lys(−2)-Arg(−1) dipeptide of the prosequence is displayed in bold.

(−1) side chain and the Asp8 or the Glu10 side chain or both, as suggested by molecular dynamics simulations. At this time, no clear experimental data has allowed us to unambiguously identify the carboxylate groups involved in this salt bridge (*1*). To clearly identify which carboxylate groups are involved in the salt bridge with the Arg(−1) side chain, we have synthesized the KR-ET-1 analogues [D8N], [E10Q], and [D18N] in which the three acidic residues were replaced one with one by the corresponding carboxamide group. Moreover, the percentages of the native and non-native disulfide patterns in these analogues were measured to demonstrate the role of each acidic residue in the formation of the native isomer (*7*). Next, assuming that the formation of the disulfide bonds occurs in a thermodynamically controlled step (*8*), we hypothesized that the salt bridge stabilizes the native structure of KR-ET-1. To confirm this hypothesis, a structural analysis of the carboxamide analogues as a function of pH was carried out. In the present work, on the basis of CD, ^{1}H NMR, and mass spectrometry data, we clearly identify the Arg(−1)−Asp8 salt bridge and demonstrate its involvement in the stability of the salt-bridged conformation and, consequently, in the formation of the native disulfide isomer of KR-ET-1. Finally, the solution structure of the minor, non-native isomer is reported and the specificity and the importance of the Arg(−1)−Asp8 salt bridge for the generation of the native isomer is discussed on a structural basis.

MATERIALS AND METHODS

Synthesis and Disulfide Bond Formation. The synthesis of KR-ET-1, its carboxamide analogues, and the non-native isomer of KR-ET-1 was carried out according to the previously described scheme (*9, 10*). Reduced peptides were obtained by treating the corresponding oxidized peptides with a 10−30-fold molar excess of dithiothreitol in 0.1 M ammonium acetate buffer at pH 9.5 for 10 min. After purification by RP-HPLC under gradient elution conditions using CH_3CN in 0.1% TFA, all the reduced peptides were stored in a freezer under a nitrogen atmosphere. Oxidative folding reactions of each peptide were carried out in the same buffer as above at pH 9.5 at a peptide concentration of 0.01 mM at 25 °C. In the case of the reaction in the presence of redox reagents, GSH and GSSG were added to the reaction medium in a ratio of 1/100/10 (peptide/GSH/GSSG). After 24 h, each reaction was analyzed by RP-HPLC on a C18 column.

Circular Dichroism. CD spectra of KR-ET-1 and its analogues were recorded at 25 °C on a JASCO J720 spectrophotometer using a 1 mm path length cell. Peptide solutions at a concentration of 0.05 mM were prepared and spectra were recorded at pH 4.0 and 1.5. Each spectrum was scanned from 195 to 250 nm and accumulated over 32 scans.

NMR Spectroscopy. (A) Sample Preparation. ^2H_2O (99.95%) was purchased from the CEA (Saclay, France). All pHs were measured in the NMR tube at room temperature with a 3-mm electrode and are given uncorrected for the deuterium isotopic effect. Lyophilized native or non-native KR-ET-1 (3 mg) was dissolved in 0.45 mL of water containing 5% ^2H_2O for the lock signal. The peptide concentration of the resulting sample was about 2.1 mM. The pH was adjusted by addition of 0.1 N HCl. TSP-d_4 was added as an internal chemical shift reference at 0 ppm. A second sample of 2 mg was prepared in 99.95% deuterated water to measure the amide proton kinetic exchange and to record spectra as a function of pH and temperature.

(B) NMR Experiments. Proton NMR experiments were performed at 300 K on two Bruker AMX spectrometers, operating at 500 and 600 MHz for ^{1}H nucleus, and data were processed with the UXNMR software. DQF-COSY (*11*), z-TOCSY (*12, 13*), NOESY (*14*), and ROESY (*15, 16*) spectra were acquired in the phase-sensitive mode using the States-TPPI method (*17*). Typically, 512 FIDs of 2048 time domain complex data points were collected, except for DQF-COSY experiments, for which better resolution was needed (800 FIDs of 4096 time domain complex data points). For spectra recorded in H_2O, except for DQF-COSY spectra (where low-power irradiation was used), the water resonance was suppressed by the WATERGATE method (*18*), in association with a water flip-back selective pulse in the NOESY spectra (*19*). The assignment of ambiguous connectivities was solved by recording spectra at two temperatures (300 and 290 K). TOCSY spectra were obtained with a mixing time of 60 ms; NOESY and ROESY spectra, with a mixing time of 200 ms. Shifted sine-bell functions were used for apodization and the data were zero-filled before processing to reach a digital resolution of 3.5 Hz/pt (600 MHz) or 2.4 Hz/pt (500 MHz) in both dimensions. The processed data were baseline corrected using a five-order polynomial function. $^3J_{NH-C\alpha H}$ coupling constants were measured by using a pulse field gradient enhanced version of DBF-COSY *(20, 21)*.

For all analogues, a set of 1D spectra was recorded in ^2H_2O at pH values ranging from 5.0 to 1.7 to check and compare the role of the ionization state of the different carboxylic acid groups.

Determination of the Free Energy Difference between the Salt-Bridged Conformation and the Salt-Bridge-Free Conformation. In the temperature range of 280−310 K and at pH 2.7, the slowly exchanging populations (in the ^{1}H NMR chemical shift time scale) of the salt-bridged and salt-bridge-free conformations for KR-ET-1 were determined by ^{1}H NMR. The population ratio was measured from the integration of the γIle19 signals and the free energy differences ΔG calculated using the equation $\Delta G = -RT \ln K$, where R is the gas constant, T is the temperature, and K is the equilibrium constant between the salt-bridged and salt-bridge-free conformations.

Mass Spectrometry. Mass spectrometry analyses of the non-native KR-ET-1 and native KR-ET-1 and its analogues were carried out on a Perkin-Elmer Sciex API III+ triple quadrupole mass spectrometer equipped with a nebulizer-assisted electrospray source. The spectra were recorded in the 450−1450 range of mass-to-charge (*m*/*z*) ratios in steps of 0.5 *m*/*z*, with a 2-ms dwell time. The signal was averaged over 10 scans. The ion spray probe tip was held at 5 kV, and the declustering voltage was set at 50 V. Samples were infused into the source using a Harvard 22 syringe pump at a flow rate of 5 μL/min.

Structure Calculations. Distance geometry calculations were carried out on a Hewlett-Packard HP735 workstation using the DIANA program (*22*) with the standard minimization parameters. Distance constraints were deduced from cross-peak intensities measured in a 200 ms NOESY experiment and were classified into four categories. Upper distance bounds of 2.5, 3.0, 4.0, and 5.0 Å were assigned to strong, medium, weak, and very weak connectivities, respectively. Lower distance bounds were taken as the sum of the van der Waals radii. As no stereospecific assignment could be made for the methyl and methylene protons, pseudoatoms were used after appropriate corrections of the constraints *(23, 24)*. Disulfide bridges were introduced through constraints of 2.0−2.1 Å on the S_i-S_j bonds and 3.0−3.1 Å on the $S_i-C\beta_j$ and $S_j-C\beta_i$ distances across the bridges. The $\chi 3$ dihedral angles were set to $\pm 80-100°$ through $C\beta_i-C\beta_j$ distance constraints of 3.75−3.95 Å. Depending on whether the $^3J_{NH-C\alpha H}$ coupling constants were high ($\geq$9.0 Hz) or low ($\leq$6.5 Hz), ϕ angles were forced between −150° and −90° and between −90° and −30°, respectively. Although several amide protons were probably involved in hydrogen bonding, because of their slow exchange, no explicit hydrogen bond constraints were included in the calculations since the carbonyls involved were not unambiguously identified. H-Bonds consistently found in the preliminary runs were explicitly introduced in the final calculations. Constraints used for distance geometry calculations of native KR-ET-1 were previously reported (*1*). For final distance-geometry calculations of non-native KR-ET-1, 160 proton−proton distances were used [62 intraresidual, 53 sequential, 17 medium range (i, $i+2$, and $i+3$) and 28 long range (i, $\geq i+4$)] along with 11 Φ angle constraints. The 20 best structures out of 1000 calculated were retained on the basis of the target function and residual distance violation values.

Energy minimizations, molecular dynamics simulations, and simulated annealing refinements were carried out with the SANDER module of the AMBER 4.1 modeling package (*25*) using the DIANA structures as a starting point as previously described (*1*). The resulting structures are hereinafter referred to as the SA structures. After fitting all SA structures to the first one (backbone atoms of residues 1−16), an average SA model was computed by coordinate averaging and refined using the same protocol applied to each individual structure. The Insight II program (Biosym Technology Inc, San Diego) was used to display and compare the structures.

Solvent-accessible surface areas were calculated for the average structures of both native and non-native KR-ET-1 with the program ACCESS (*26*) using a sphere probe radius of 1.4 Å. Side-chain atomic areas were grouped according to polar (N, O) or apolar (C, S) atom types leading to polar and apolar side-chain surface areas. The percentage of accessibility for each side chain was calculated from the difference between total (polar and apolar) side-chain surface areas in the protein and in model tripeptides (*27*).

RESULTS AND DISCUSSION

I. Identification of the Highly Specific Arg(−1)−Asp8 Salt Bridge That Stabilizes the Structure of Native KR-ET-1

The previously reported KR-ET-1 solution structure is characterized by a conformational change of the N- and C-terminal parts that depends on the ionization state of the carboxyl groups (*1*). In the carboxylic acid state, the C-terminal part (fragment 16−21) appeared typically unstructured. In the carboxylate state, a salt bridge involving Arg(−1) was formed, resulting in a more structured N-terminal part. A concomitant more structured C-terminal part was also observed leading to an extension of the helical part up to Leu17 in agreement with the increase in the helical content observed on CD spectra at pH 4.0. In the following text, unless stated otherwise, KR-ET-1 will refer to the native disulfide bond isomer, and the carboxylate state and carboxylic acid state conformations will be referred to as the salt-bridged conformation and the salt-bridge-free conformation, respectively.

Structural Studies of the [D8N], [E10Q], and [D18N] Analogues of KR-ET-1. The [D8N], [E10Q], and [D18N] analogues of KR-ET-1 were synthesized to determine which carboxylate groups are involved in the salt bridge with Arg(−1). Such replacements selectively remove one negative charge and, consequently, abolish the salt bridge with the mutated residue. As previously reported for the parent peptide, the structural studies of the analogues were based on CD and ^{1}H NMR data obtained at pH values ranging from 1.5−1.7 to 5.0 (*1*).

(A) Circular Dichroism. CD spectra were recorded at pH 1.5 and 4.0, to track the conformational changes between the carboxylic acid and carboxylate states (*7*) (Figure 2). At pH 1.5, the CD spectra of ET-1 and of KR-ET-1 and its [D8N], [E10Q], and [D18N] analogues were similar, with an absorption minimum around 206−207 nm. At pH 4.0, spectra of KR-ET-1 and of the analogues [E10Q] and [D18N] were similarly modified, and all displayed a shoulder at 222 nm, suggesting a higher helical content. For ET-1 and for the [D8N] analogue, similar CD spectra were observed at pH 1.5 and 4.0. Clearly, the [D8N] analogue displays the same behavior as ET-1. The fact that the spectrum of the [D8N] analogue remains unchanged as a function of pH, in contrast to those of KR-ET-1 and the [E10Q] and [D18N] analogues, suggests that the Asp8 side chain is specifically salt bridging with Arg(−1).

(B) NMR of the [D8N], [E10Q], and [D18N]-KR-ET-1 Analogues. The ^{1}H NMR spectra of KR-ET-1 in the 1.7−5.0 pH range showed that the nonexchangeable protons of Tyr13, Phe14, Ile19, and His16 residues displayed typical chemical shifts in the salt-bridged (pH 5.0) and salt-bridge-free (pH 1.7) conformations (*1*). The reversible conformational change between these two conformations is directly dependent on the ionization state of carboxyl groups. Furthermore, due to the slow exchange on the ^{1}H NMR

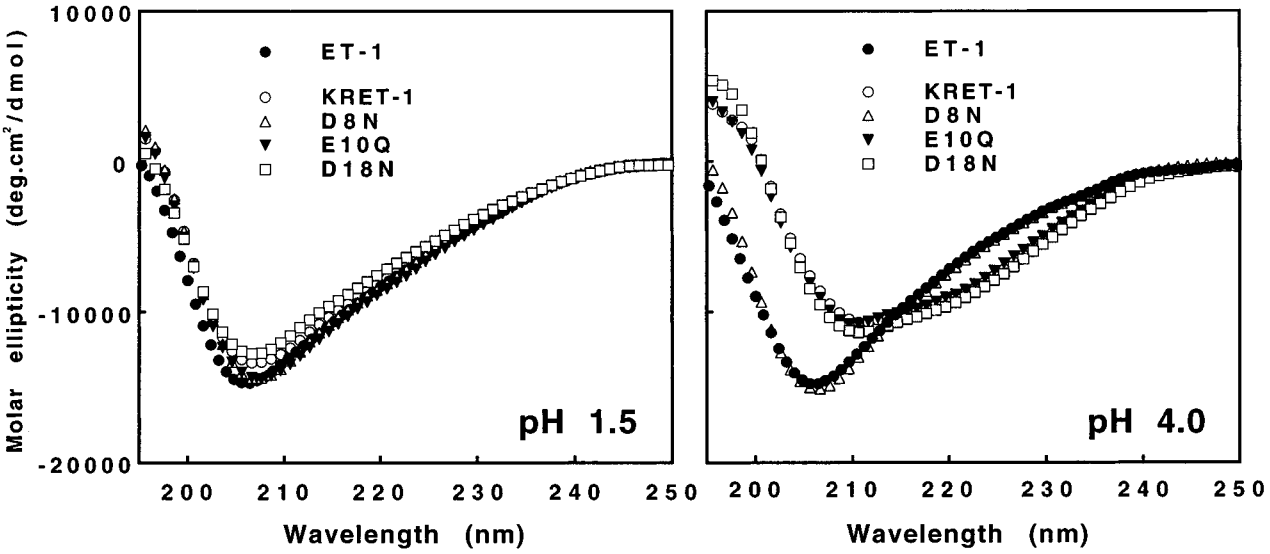

FIGURE 2: CD spectroscopic study of the pH-induced conformational change of ET-1 and of KR-ET-1 and its three analogues [D8N], [E10Q], and [D18N] displaying the native disulfide bond pattern recorded at pH 1.5 and 4.0. Spectra of KR-ET-1, [D18N], and [E10Q] display a similar conformational change. In contrast, ET-1 and [D8N] spectra are practically insensitive to the ionization state of the carboxyl groups.

chemical shift time scale between the salt-bridged and salt-bridge-free conformations, the two typical spectra were simultaneously observed at intermediate pH values. The integration of γIle19 signals was used as a conformational probe to follow the evolution of the conformational change during the pH titration and the variation of temperature.

The spectra of the [D8N], [E10Q], and [D18N] analogues were recorded in deuterated medium in the 1.7−5.0 pH range. The sets of 1D spectra recorded with the [E10Q] analogue (Figure 3A) and with the [D18N] analogue (spectra not shown) are very similar to that obtained with KR-ET-1. As for KR-ET-1, almost pure salt-bridged and salt-bridge-free conformations were observed at pH 5.0 and 1.7, respectively. For intermediate pH values, γIle19, Tyr13, Phe14, and His16 signals clearly showed the gradual transformation of one conformation to the other. In contrast, in the same pH range, unchanged spectra were obtained for the [D8N] analogue (Figure 3B). In these spectra, chemical shifts of γIle19, Tyr13, Phe14, and His16 signals were typically those of the salt-bridge-free conformation. This pH independence of the NMR spectra of the [D8N] analogue is indicative of the major role played by the Asp8 carboxylate group in the conformational change exhibited by KR-ET-1 and the [E10Q] and [D18N] analogues.

Taken together, the CD and NMR spectral changes as a function of pH demonstrate that the Asp8 carboxylate group interacts with Arg(−1). The resulting highly specific Arg(−1)−Asp8 salt bridge appears to be responsible for the conformational change observed for KR-ET-1 and the [E10Q] and [D18N] analogues since it depends on the ionization state of the Asp8 carboxyl group. Moreover, the involvement of Asp8 in salt bridging with Arg(−1) is consistent with the large nonequivalence observed between the Cβ protons of Asp8 (1.07 ppm) in the NMR spectra of KR-ET-1 recorded at pH 4.1 (*1*). It is noteworthy that this large nonequivalence, probably due to the conformational constraints introduced by the salt bridge interaction, is significantly reduced at pH 1.7 (0.24 ppm) when the Arg(−1)−Asp8 salt bridge is disrupted by protonation of the Asp8 carboxylate group to give the salt-bridge-free conformation (Figure 3A).

Relative Stability of the Salt-Bridged and Salt-Bridge-Free Conformations of KR-ET-1. To evaluate the relative stability of the salt-bridged and salt-bridge-free conformations of KR-ET-1, a set of 1D spectra was recorded as a function of temperature from 280 to 345 K and at pH 2.7 (Figure 4). At low temperature (280 K), the equilibrium is highly displaced toward the most stable conformation, i.e., the salt-bridged conformation, and the kinetics of the exchange is slow on the ^{1}H NMR chemical shift time scale. As the temperature was increased to 310 K, the two conformations became equally populated. At higher temperature (310−325 K), the salt-bridge-free conformation became the major conformation and an intermediate exchange regime responsible for the line broadening was reached. Above 330 K, fast exchange conditions were gradually reached, resulting in sharp signals. At 340 K the spectrum was typically that of the pure salt-bridge-free conformation.

At 300 K, signals indicative of each conformation were simultaneously observed (Figure 4). The equilibrium constant between the salt-bridged and salt-bridge-free conformations was determined from the integration of the corresponding γIle19 signal (K_{eq} = [salt-bridged conformation]/[salt-bridge-free conformation]). At 300 K and at pH 2.7, the salt-bridged conformation is favored by 0.53 kcal/mol ($\Delta G = -RT \ln K_{eq}$; $K_{eq} = 2.4$). This value has to be compared with values ranging from 0.5 to 5 kcal/mol reported in the literature for salt bridge stabilizations (*28*−*34*).

II. Role of the Arg(−1)−Asp8 Salt Bridge in KR-ET-1 Folding

Formation of Disulfide Bonds of KR-ET-1 Analogues. To demonstrate the potential role of the Arg(−1)−Asp8 salt bridge in the formation of native disulfide bonds, the ratio of native to non-native disulfide isomers was measured for [E10Q] and [D18N], which bear the Arg(−1)−Asp8 salt bridge, and for the [D8N] analogue for which the native

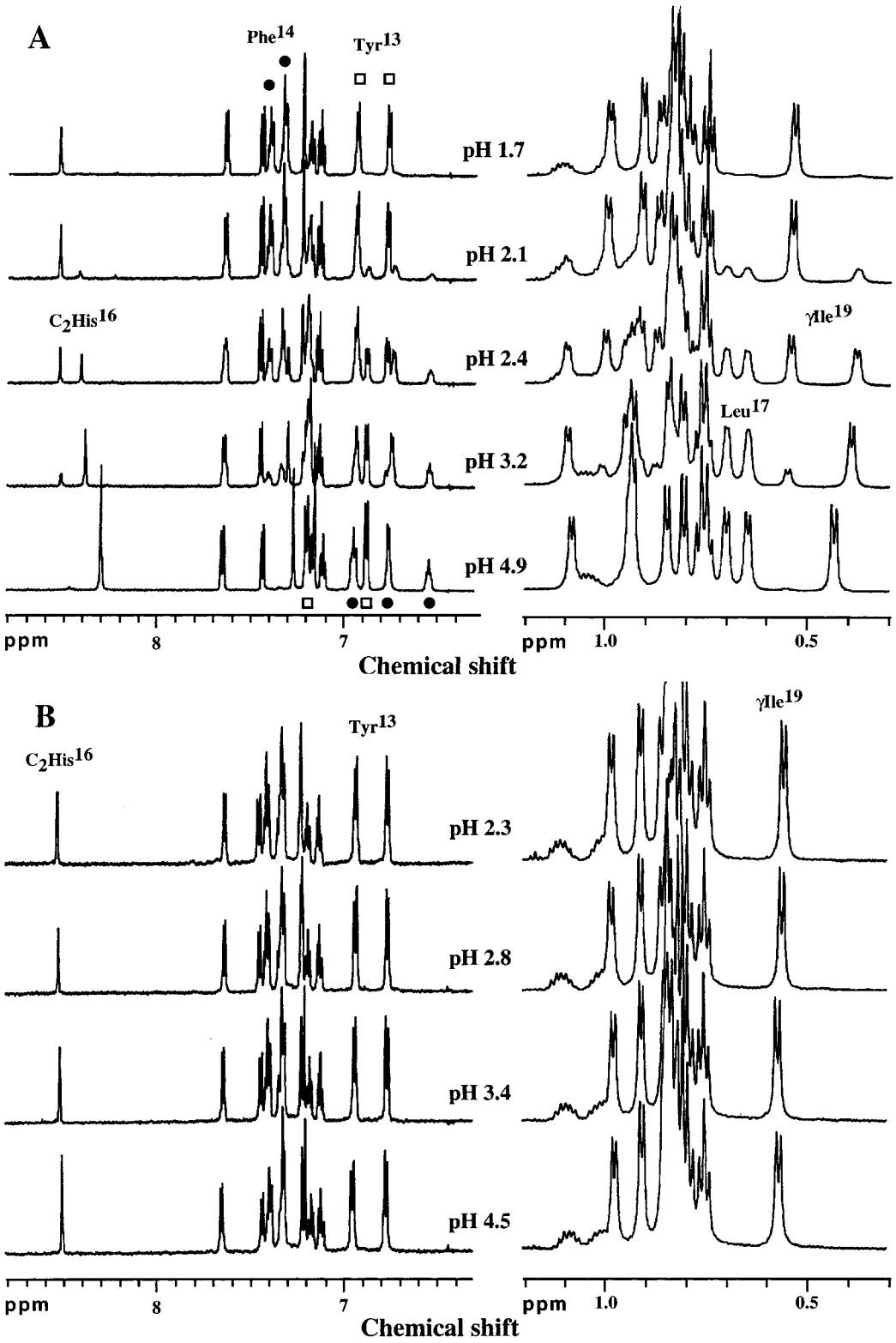

FIGURE 3: Aromatic and methyl signal areas of ^{1}H NMR spectra of [E10Q] (A) and [D8N] (B) analogues recorded in deuterated water from pH 1.5 to 5.0 at 300 K. (A) The low-field (0.55 ppm, 300 K) and high-field (0.41 ppm) signals of γIle19 of the [E10Q] analogue are characteristic of the salt-bridge-free and salt-bridged conformations, respectively. Similar pH-induced spectral changes were observed with KR-ET-1 and with the [D18N] analogue. Y13 and F14 aromatic signals are labeled by open boxes and filled circles, respectively, both on the spectrum typical of the salt-bridged conformation (pH 4.9) and on the spectrum typical of the salt-bridge-free conformation (pH 1.7). (Part B) In contrast to what we observed for KR-ET-1 and the [E10Q] and [D18N] analogues, the spectra of the [D8N] analogue are unchanged whatever the pH value in the same pH range.

isomer is unable to form the Arg(−1)−Asp8 salt bridge (Table 1) (*7*). The yield of the native disulfide isomer of KR-ET-1 is significantly higher than that of ET-1 (88/12 vs 75/25) and is further increased to 96/4 by addition of redox reagents. [E10Q] and [D18N] analogues display roughly the same ratio of native to non-native isomers (≥90/10). In contrast, the [D8N] analogue displayed a native to non-native ratio of 68/32, close to that measured for ET-1 (≈71/29).

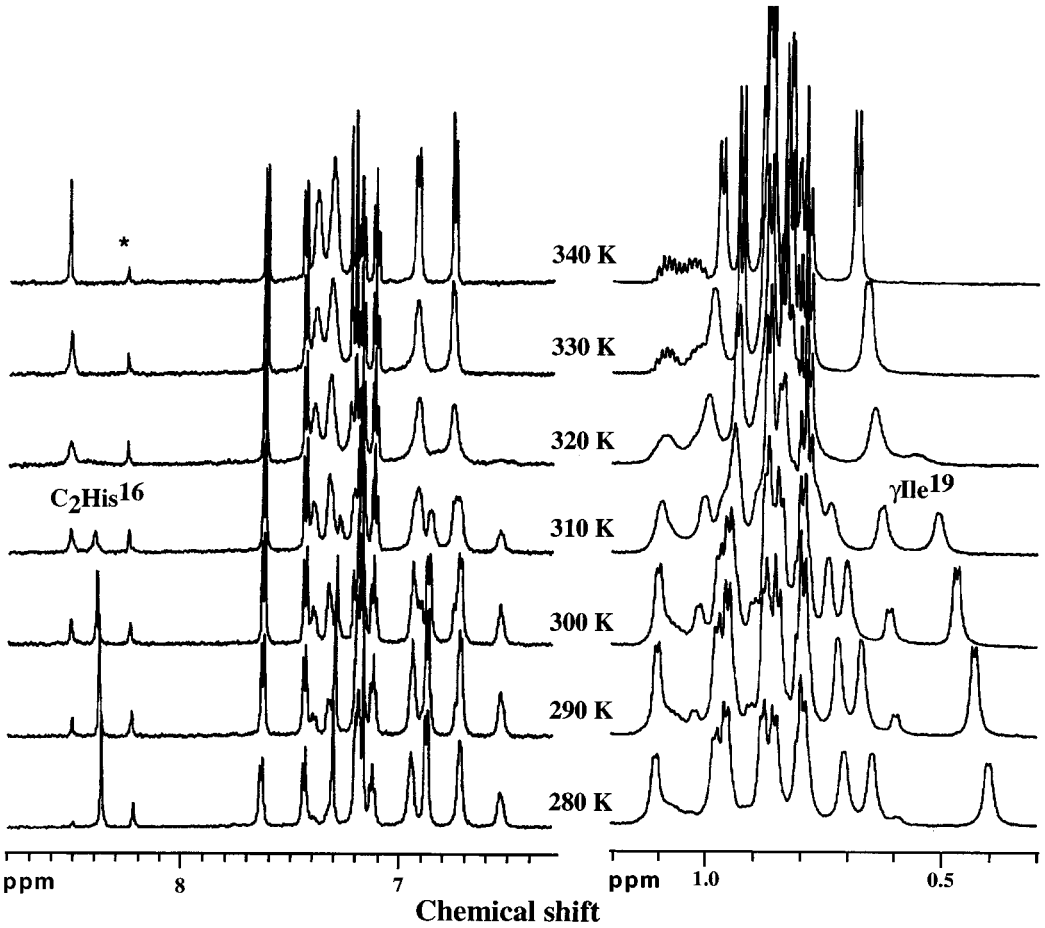

FIGURE 4: Low- and high-field regions of the KR-ET-1 spectra recorded at different temperatures ranging from 280 to 345 K (pH 2.7 in D_2O). For the sake of clarity only seven spectra are displayed. Spectra recorded at 280 and 340 K are typically those of the salt-bridged and salt-bridge-free conformations, respectively. The two conformations are unambiguously identified from the characteristic chemical shifts of γIle19, from C_2H of His16, and from the Tyr13 and Phe14 aromatic signals. At an intermediate temperature (310 K), the two spectra of equal intensity that correspond to each conformation are observed simultaneously, due to the slow exchange conditions. Notice the line broadening at 320 K due to the rate increase of the conformational exchange and the sharp lines at 340 K when fast exchange conditions were reached. The asterisk indicates an impurity peak.

Table 1: Ratios of Native to Non-Native Disulfide Bond Isomers Measured in the Oxidative Step of ET-1, KR-ET-1, and Its Carboxamide Analogues in the Presence and in the Absence of the Redox Couple GSH/GSSG[a]

analog	without GSH/GSSG	with GSH/GSSG
ET-1	75/25	71/29
KR-ET-1	88/12	96/4
[D8N]-KR-ET-1	66/34	68/32
[E10Q]-KR-ET-1	88/12	94/6
[D18N]-KR-ET-1	80/20	90/10

[a] The percentage of the two isomers was measured by integration of the corresponding HPLC signal.

The fact that KR-ET-1 and the [E10Q] and [D18N] analogues, which all display the Arg(−1)−Asp8 salt bridge, gave high yields of native disulfide bonds, together with the fact that the [D8N] analogue, which did not display such a salt bridge, gave a native to non-native ratio similar to that of ET-1, strongly supports the direct involvement of the Arg(−1)−Asp8 salt bridge in the improved formation of the native disulfide bonds.

The disulfide bond isomers are usually supposed to be formed in a thermodynamically controlled step (*8*). Indeed, starting from either pure native or pure non-native KR-ET-1 isomers under conditions allowing disulfide rearrangement (i.e., pH 9.5 in the presence of the redox reagents), an equilibrium close to that observed for the oxidative folding of the reduced KR-ET-1 was reached, namely, a ratio of 96/4 (data not shown). Thus, it is likely that the improvement of the native to non-native ratio observed for KR-ET-1, when compared with that of ET-1, was due to an extra stabilization of the native isomer by the Arg(−1)−Asp8 salt bridge, which is absent or weaker in the non-native isomer. To gain support for this hypothesis, we decided to determine the solution structure of the non-native isomer of KR-ET-1 and evaluate its salt bridge potentialities.

Solution Structure of the Non-Native KR-ET-1 Isomer and Comparison with the Structure of Native KR-ET-1. The salt bridge potentialities of the synthetic non-native isomer of KR-ET-1 were studied using mass spectrometry, and its structure was determined by using CD and ^1H NMR experiments.

The electrospray ionization mass spectrometry method (ESIMS) was used to check the salt bridge potentialities of the non-native isomer of KR-ET-1 in comparison with KR-ET-1 and its analogues described above. Indeed, by using soft ionization conditions, this method allows noncovalent interactions to remain intact and to be observed. Consequently, from variations of the relative intensity of the

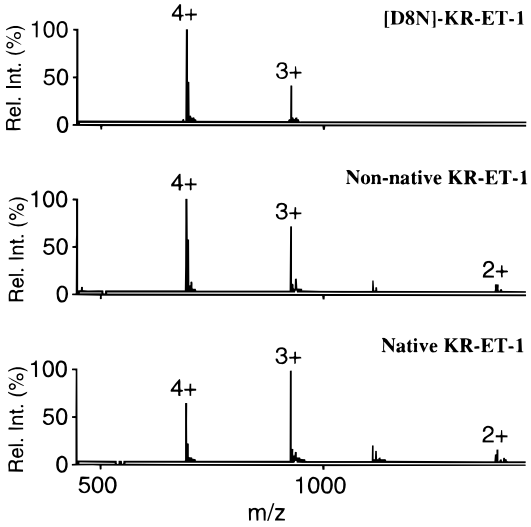

FIGURE 5: Electrospray mass spectra of native KR-ET-1, its [D8N] analogue, and the non-native KR-ET-1 recorded from pH 4.2 solutions. At pH 1.8, these three compounds give similar spectra in which the 4+ is the major signal (data not shown). At pH 4.2, [D8N] and non-native KR-ET-1 give unchanged spectra, suggesting that there is not any strong salt bridge. In contrast, for native KR-ET-1 the loss of one positive charge is indicative of its involvement in the strong salt bridge identified on the basis of the CD and NMR results. The [E10Q] analogue displays the same behavior as native KR-ET-1 (spectrum not shown).

different positively charged signals of the spectrum, the presence or the absence of a stable salt bridge should be detected. Therefore, spectra of the [D8N] and [E10Q] analogues and of native and non-native isomers of KR-ET-1 were recorded from pH 1.8 and 4.2 solutions. All spectra from pH 1.8 solutions displayed the 4+ signal as the most important one (data not shown). As expected, from pH 4.2 solutions the 3+ signal was the most important for native KR-ET-1 and for the [E10Q] analogue in agreement with the involvement of a positive charge Arg(−1) in a stable salt bridge with the Asp8 carboxylate group, whereas an unchanged spectrum was obtained for the [D8N] analogue, due to the absence of this stable salt bridge (Figure 5) as shown. Concerning the non-native isomer of KR-ET-1, the fact that at the two pH values the 4+ signal remained the most important suggests the absence of a stable salt bridge. Although quantitative analysis of these results has to be considered with caution, the tendency is consistent with the data reported above for native KR-ET-1 and the [D8N] and [E10Q] analogues. In this case, ESIMS appeared to be a valuable technique to quickly detect the presence or the absence of a stable salt bridge, and as far as we know, this is the first application of this technique to salt bridge detection in peptides.

As for the native isomer, to identify potential stable salt bridges involving Lys(−2) or Arg(−1) side chains of the non-native isomer, CD and NMR spectra were recorded as a function of pH. CD spectra of non-native ET-1 and of non-native KR-ET-1 recorded at pH 1.5 and 4.0 were very similar, suggesting that the peptides possess similar structures (Figure 6). In addition, the pH independence of CD spectra of the non-native KR-ET-1 isomer is indicative of the absence of a structural change induced by deprotonation of carboxyl groups, contrary to that which we observed for the native isomer. 2D NMR data sets of non-native KR-ET-1 were recorded at pH 1.8, 3.7, and 5.2, and the full assignment was performed according to the strategy described by Wüthrich, (*24*).

Given that Hα chemical shifts are in part representative of secondary structures, they were analyzed according to the chemical shift index (CSI) method (*35*−*37*). Such an analysis carried out for the two isomers (Figure 7) revealed an upfield tendency in the region extending from K9 to C15 suggesting a helical structure. Nevertheless, when Hα chemical shifts of the two isomers were compared, the largest differences were observed for the C1−S5 section and for C11 and F14 residues, suggesting a structural change of the C1−C15 part of the molecule, probably due to the different disulfide arrangement. Most interestingly, only one spectrum was observed in the 1.8−5.2 pH range, and ROESY experiments did not show any exchange cross-peak that could reveal the presence of a minor conformation. Moreover, in this pH range the chemical shifts of NεH and Cδ2H of Arg(−1) displayed standard values (7.15 and 3.12 ppm, respectively), in contrast to the large chemical shift differences observed for these signals for the native isomer. Chemical

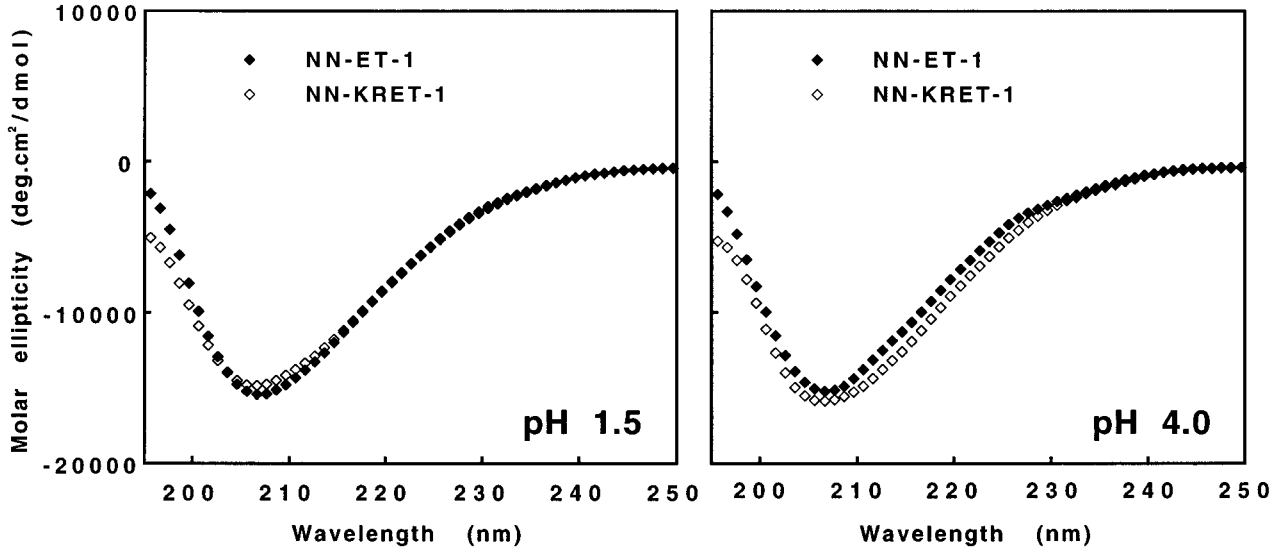

FIGURE 6: CD spectra of the non-native isomers of ET-1 and KR-ET-1 recorded at pH 1.5 and 4.0. The spectra are insensitive to the ionization state of the carboxyl groups.

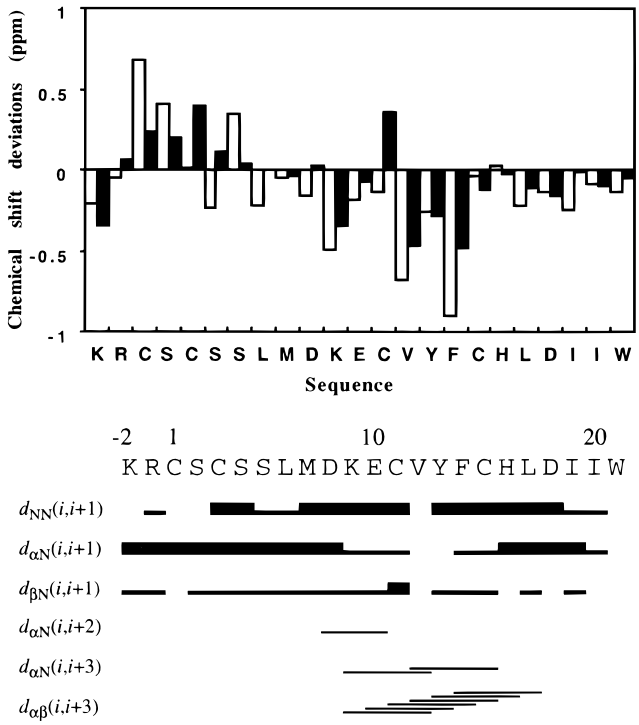

FIGURE 7: (Top) Chemical shift deviations of Hα protons (CSI) calculated for native (open bars) and non-native (closed bars) isomers of KR-ET-1. (Bottom) Summary of NOEs measured for the non-native isomer of KR-ET-1 (300 K, pH 3.7).

shifts of protons of the Lys(−2) side chain also remained unchanged. These observations clearly indicate that no salt bridge involving the N-terminal basic dipeptide was experimentally observed for the non-native isomer and that its solution structure is independent of the ionization state of carboxyl groups.

Distance geometry calculations of non-native KR-ET-1 based on NMR-derived distance constraints, $^3J_{HN-C\alpha H}$ coupling constants, and hydrogen bonding measured at pH 3.7 (Figure 7) were carried out. The 20 best structures were further refined by restrained simulated annealing calculations and are displayed in Figure 8 along with an average structure. The average structure of the non-native isomer was compared with that of the native isomer as determined in the carboxylate state and clearly shows a good conservation of the helical portion (Figure 9). The two structures markedly differ about the orientation of the KRCSC backbone. In the native isomer, this section belongs to an extended strand lying roughly antiparallel to the helix, whereas in the non-native isomer it is approximately perpendicular to the helix, and the Lys(−2) and Arg(−1) side chains are solvent exposed.

III. Disulfide Bond Formation and Specificity of the Arg(−1)−Asp8 Salt Bridge for the Native Isomer: Hydrophobic Interactions and Helix Stability

Given that the disulfide bonds are usually formed in a thermodynamically controlled step, free energy differences of ∼−0.64 kcal/mol and −1.28 kcal/mol between the non-native and native structures were calculated on the basis of the ratio of native to non-native isomers for ET-1 (ratio 3/1) and for KR-ET-1 (ratio 9/1), respectively. Figure 10 shows hypothetical energy levels of native and non-native isomers of ET-1 and of KR-ET-1. For native KR-ET-1, due to the pH-dependent conformational change, two energy levels have to be considered, one corresponding to the salt-bridge-free conformation (level displayed as a dashed line in Figure 10) and the other corresponding to the salt-bridged conformation. Only the latter conformation has to be considered at physiological pH or under conditions used for the oxidative folding in the chemical synthesis.

We have demonstrated on the basis of CD a structural similarity between the native isomer of ET-1 and the salt-bridge-free conformation of native KR-ET-1, both displaying an unstructured C-terminal part. Similarly, on the basis of the CD spectra of the non-native ET-1 and the non-native KR-ET-1, isomers appeared structurally similar in the 1.5−4.0 pH range (Figure 6). Therefore, in the absence of specific interactions, the free energy difference between the non-native KR-ET-1 structure and the native salt-bridge-free KR-ET-1 conformation is supposed to be close to the free energy difference measured between native and non-native isomers of ET-1 (∼−0.64 kcal/mol). However, under conditions where the salt-bridged conformation largely predominates (pH 9.5), a free energy difference of −1.28 kcal/mol was calculated between native and non-native KR-ET-1 isomers. This larger value of ΔG between native and non-native isomers of KR-ET-1 (−1.28 kcal/mol instead of −0.64 kcal/mol for ET-1) is probably mainly due to stabilization of the native isomer by the Arg(−1)−Asp8 salt bridge, i.e., to the difference in stability between the salt-bridge-free and salt-bridged conformations. Thus, the native isomer would be preferentially formed in the thermodynamically controlled step.

During simulated annealing calculations, it appeared that distances between the Arg(−1) guanidinium group and the Asp8 or Glu10 carboxylate groups in several conformations were compatible with salt bridge formation. However, in these conformations salt bridges are probably not stable enough to be experimentally observed. This is in agreement with the fact that salt bridges exposed to the solvent have a weak effect on protein stability (*39*−*40*), compared with buried salt bridges (*41*). The fact that the salt bridge is only observed in the native structure highlights its specificity and suggests that to stabilize the conformation of native KR-ET-1 in water, in addition to the Arg(−1)−Asp8 salt bridge, other associated interactions must also take place and contribute in a cooperative manner to the stabilization of the salt-bridged conformation. Indeed, taking into account that the Arg(−1) side chain displays an amphiphilic character and that it is located close to the hydrophobic cystine-stabilized motif, some stabilizing hydrophobic interactions are expected. The involvement of the Arg(−1) side chain in hydrophobic interactions was clearly supported by the fact that only 18% of its apolar surface was accessible to the solvent in the salt-bridged conformation, whereas it is fully exposed in the non-native isomer. Therefore, due to its ability to be involved in both electrostatic and hydrophobic interactions (*42*−*44*), the Arg(−1) residue plays a major role in the stability of the salt-bridged conformation of the native structure of KR-ET-1. On the other hand, for the non-native isomer, the orientation of the KRCSC segment probably does not favor generation of enough cooperativity between electrostatic and hydrophobic interactions to stabilize salt bridges involving the Lys(−2) or Arg(−1) side chains. As

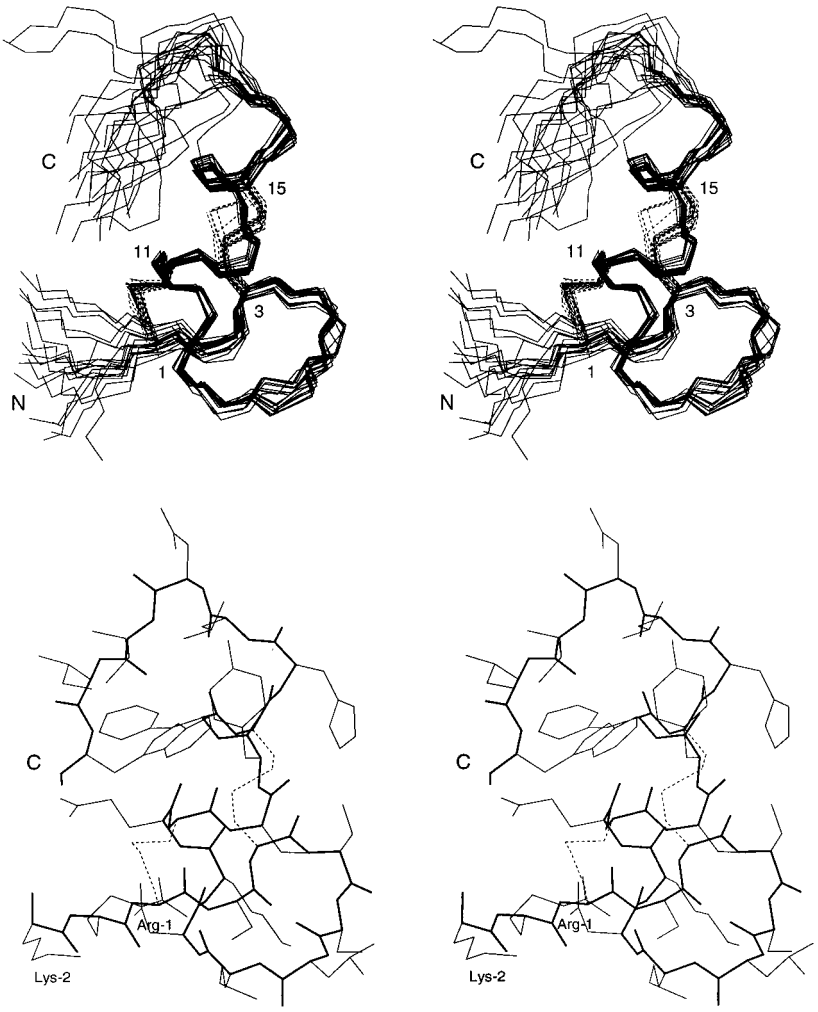

FIGURE 8: Stereoviews of the structures of the non-native KR-ET-1 isomer as determined from NMR constraints (pH 3.7). (Top) Backbone atoms (N, Cα, C) and disulfide bridges (dashed lines) of the 20 best simulated annealing structures. Residues 1−16 were used for the superimposition. (Bottom) Average simulated annealing structure. The backbone, side chains, and disulfide bonds are shown as thick, thin, and dashed lines, respectively. The Lys(−2) and Arg(−1) side chains are exposed to the solvent.

a result, without such additional stabilizing interactions, the oppositely charged side chains remain mobile in the non-native isomer and no specific electrostatic interaction can be experimentally observed. We conclude that the folding improvement in KR-ET-1, versus ET-1, is a direct consequence of the additional stability afforded by the salt bridge in native KR-ET-1, in comparison with the non-native isomer whose structure does not allow efficient cooperativity between the electrostatic and hydrophobic interactions.

The Arg(−1)−Asp8 salt bridge was expected to contribute mainly to the stability of the N-terminal part in the region of Arg(−1) and of the N-terminal part of the helix in the region of Asp8. But surprisingly, reduced mobility of the hydrophobic C-terminal part (fragment 16−21) was also observed. We think that this might result from hydrophobic interactions due to the buried Arg(−1) side chain. These hydrophobic interactions contribute to the helix stability and to its extension up to Leu17 in agreement with the higher helix content clearly observed on CD spectra of compounds able to display the Arg(−1)−Asp8 salt bridge (Figure 2).

In comparison with data obtained in the study on the disulfide bond formation in ET-1, helix stabilization seems to be related to the yield of native disulfide bond isomer. This is supported by the high yield of the native disulfide isomer (≥95%) measured for the [Y13A]-ET-1 analogue (*45*) since the Ala residue has a high helix forming tendency (*46*, *47*, *31*). In contrast, the same substitution by a D-Ala residue, which does not favor helical structures (*48*), yielded only 50% of the native isomer (*49*). Furthermore, when the oxidation of ET-1 was carried out in the presence of trifluoroethanol (water−TFE, 1:1), a well-known helix inducer, 88% (*7*) and even 91% (*50*) of the native disulfide isomer was formed. Taken together, all these data suggest a close relationship between the helix stability and the yield of the native disulfide bonded isomer.

In the porcine or human endothelin precursors, the fragment 53−73 corresponds to the endothelin sequence, whereas the fragment 1−19 corresponds to the signal peptide (*51*). Interestingly, the propeptide fragment spanning residues 20−52 contains 30% charged residues (5 Glu, 4 Arg, and 1 Lys). Several propeptides with such a high content of charged residues have been proposed to play a significant role in the folding of several proteins, such as α-lytic protease, subtilisin, carboxypeptidase Y, and BPTI, and this effect has sometimes been referred to as intramolecular chaperoning (*52*−*55*). The high content of basic residues in the C-terminal part of the endothelin propeptide (RXRR-SKR, X = P or L) is particularly remarkable. We have

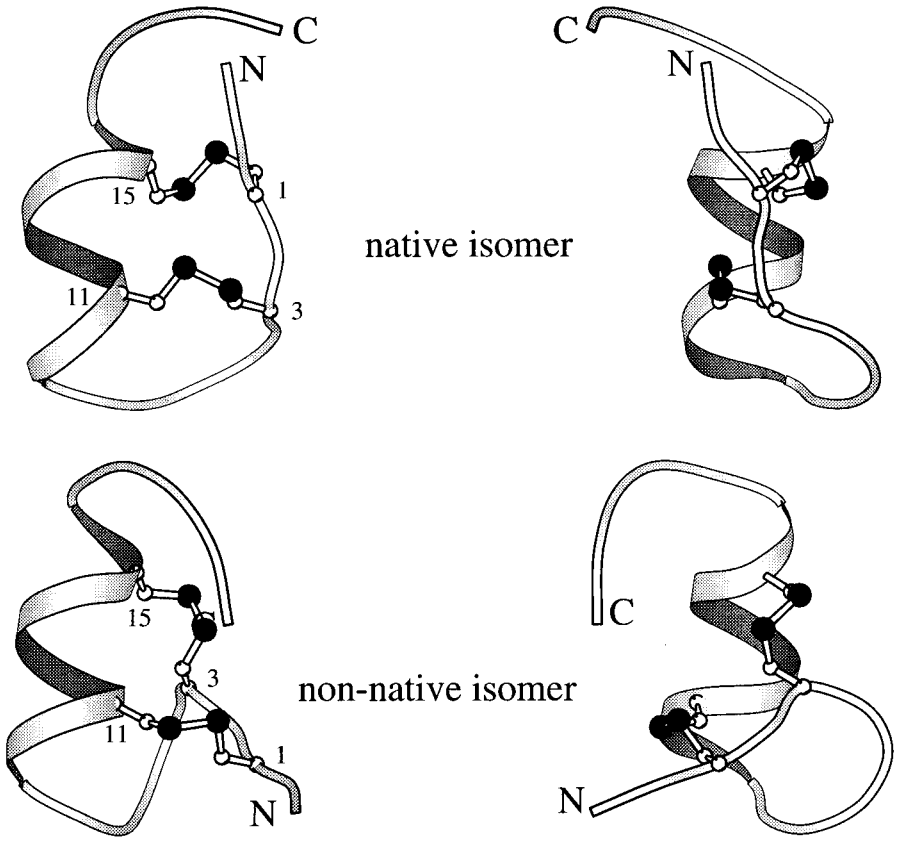

FIGURE 9: Two views, 90° apart, of the native and non-native KR-ET-1 isomers, top and bottom, respectively. The two isomers differ from the disulfide pattern. The orientation of the KRCSC sequence is quite different in the two isomers. The sequence that is antiparallel to the helix in native KR-ET-1 becomes almost perpendicular in the non-native isomer. The views were prepared with MOLSCRIPT (*38*).

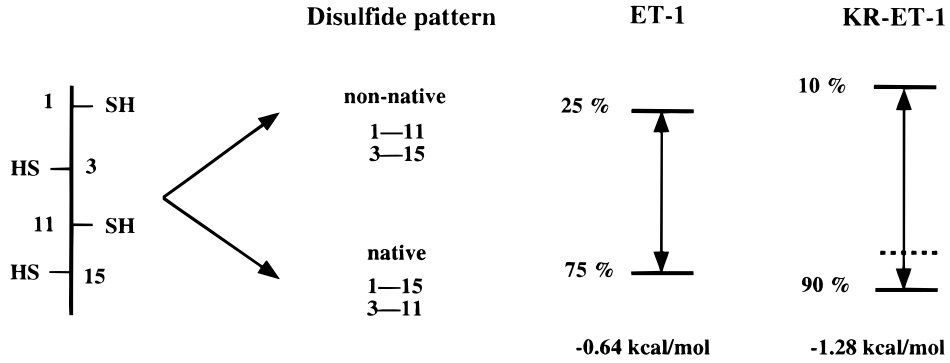

FIGURE 10: Scheme displaying the yield in native and non-native disulfide bond isomers for ET-1 and KR-ET-1 in water, hypothetical energy levels of ET-1 and KR-ET-1 isomers, and free energy differences calculated from the ratio of native to non-native isomers at 293 K for ET-1 and KR-ET-1. The dashed line corresponds to the hypothetical energy level of the nonstabilized conformation of KR-ET-1.

shown that electrostatic interactions between the propeptide and the protein sequence in endothelin play a significant role in the oxidative folding process, suggesting that similar effects might occur in other cases, too. It could be hypothesized that the highly specific Arg(−1)−Asp8 salt bridge was selected by evolution to help the in vivo folding before the maturation process. A better knowledge of these kinds of interactions should be useful to improve our understanding of the in vitro folding of synthetic or over-expressed proteins.

ACKNOWLEDGMENT

A.A. would like to thank the Institute for Protein Research of Osaka University and the Peptide Institute, Inc., Protein Research Foundation, Japan, for facilities provided during his stay in 1996. The authors are indebted to Dr. S. L. Salhi for the editorial revision of the manuscript.

REFERENCES

1. Aumelas, A., Chiche, L., Kubo, S., Chino, N., Tamaoki, H., and Kobayashi, Y. (1995) *Biochemistry 34*, 4546−4561.
2. Tamaoki, H., Kyogoku, Y., Nakajima, K., Sakakibara, S., Hayashi, M., and Kobayashi, Y. (1992) *Biopolymers 32*, 353−357.
3. Tamaoki, H., Kobayashi, Y., Nishimura, S., Ohkubo, T., Kyogoku, Y., Nakajima, K., Kumagaye, S., Kimura, T., and Sakakibara, S. (1991) *Protein Eng. 4*, 509−518.
4. Kobayashi, Y., Takashima, H., Tamaoki, H., Kyogoku, Y., Nakajima, K., Lambert, P., Kuroda, H., Chino, N., Watanabe, T. X., Kimura, T., Sakakibara, S., and Moroder, L. (1991) *Bioplymers 31*, 1213−1220.

5. Mihara, H., Tomizaki, K., Nishino, N., Fujimoto, T, Tamaoki, H., and Kobayashi, Y. (1994) *Biopolymers 34*, 963−967.
6. Aumelas, A., Chiche, L., Mahé, E., Le-Nguyen, D., Sizun, P., Berthault, P., and Perly, B. (1991) *Int. J. Pept. Protein Res. 37*, 315−324.
7. Kubo, S., Chino, N., Nakajima, K., Aumelas, A., Chiche, L., Segawa, S., Tamaoki, T., Kobayashi, Y., Kimura, T., and Sakakibara, S. (1997) *Lett. Pept. Sci. 4*, 185−192.
8. Gilbert, H. F. (1994) in *Mechanisms of Protein Folding* (Pain, R. H., Ed.) pp 104−136, IRL Press, Oxford.
9. Nakajima, K., Kubo, S., Kumagaye, S., Nishio H., Kuroda, H., Tsunemi, M., Inui, T., Kuroda, H., Chino, N., Watanabe, T. X., Kimura, T., and Sakakibara, S. (1989) *Biochem. Biophys. Res. Commun. 163*, 424−429.
10. Kumagaye, S., Kuroda, H., Nakajima, K., Watanabe, T., Kimura, T., Masaki, T., and Sakakibara, S. (1988) *Int. J. Pept. Protein Res. 32*, 519−526.
11. Rance, M., Sorensen, O. W., Bodenhausen, G., Wagner, G., Ernst, R. R., and Wüthrich, K. (1983) *Biochem. Biophys. Res. Commun. 117*, 479−485.
12. Bax, A., and Davis, D. G. (1985) *J. Magn. Reson. 65*, 355−360.
13. Rance, M. (1987) *J. Magn. Reson. 74*, 557−564.
14. Macura, S., Huang, Y., Sutter, D., and Ernst, R. R. (1981) *J. Magn. Reson. 43*, 259−281.
15. Bax, A., and Davis, D. G. (1985) *J. Magn. Reson. 63*, 207−213.
16. Dezheng, Z., Fujiwara, T., and Nagayama, K. (1989) *J. Magn. Reson. 81*, 628−630.
17. Marion, D., Ikura, M., Tschudin, R., and Bax, A. (1989) *J. Magn. Reson. 85*, 393−399.
18. Piotto, M., Saudek, V., and Sklenar, V. (1992) *J. Biomol. NMR 2*, 661−665.
19. Lippens, G., Dhalluin, C., and Wieruszeski, J. M. (1995) *J. Biomol. NMR 5*, 327−331.
20. Roumestand, C., Mispelter, J., Austruy, C., and Canet, D. (1995) *J. Magn. Reson. B109*, 153−164.
21. Roumestand, C., Mutzenhart, P., Delay, C., and Canet, D. (1996) *Magn. Reson. Chem. 34*, 807−814.
22. Günther, P., Braun, W., and Wüthrich, K. (1991) *J. Mol. Biol. 217*, 517−530.
23. Wüthrich, K., Billeter, M., and Braun, W. (1983) *J. Mol. Biol. 169*, 949−961.
24. Wüthrich, K. (1986) in *NMR of Proteins and Nucleic Acids*, John Wiley and Sons, New York.
25. Pearlman, D. A., Case D. A., Caldwell, J. C., Ross, W. S., Cheatham, T. E., Ferguson, D. M., Seibel, G. L., Chandra Singh, U., Weiner, P., and Kollman, P. A. (1995) *AMBER*, version 4.1, University of California, San Francisco.
26. Richmond, T. J., and Richards, F. M. (1978) *J. Mol. Biol. 119*, 537−555.
27. Shrake, A., and Rupley, J. A. (1973) *J. Mol. Biol. 79*, 351−371.
28. Creighton, T. E. (1993) in *Proteins, Structures and Molecular Properties*, 2nd ed., p 293, W. H. Freeman and Co., New York.
29. Anderson, D. E., Becktel, W. J., and Dahlquist, F. W. (1990) *Biochemistry 29*, 2403−2408.
30. Sun, D. P., Sauer, U., Nicholson, H., and Matthews, B. W. (1991) *Biochemistry 30*, 7142−7153.
31. Bryson, J. W., Betz, S. F., Lu, H. S., Suich, D. J., Zhou, H. X., O'Neil, K. T., and De Grado, W. F. (1995) *Science 270*, 935−941.
32. Lyu, P. C., Gans, P. J., and Kallenbach, N. R. (1992) *J. Mol. Biol. 223*, 343−350.
33. Tissot, A. C., Vuilleumier, S., and Fersht, A. R. (1996) *Biochemistry 35*, 6786−6794.
34. Kallenbach, N. R., Lyu, P., and Zhou H. (1996) in *Circular Dichroism and the Conformational Analysis of Biomolecules* (Fasman, G. D., Ed.) pp 201−260, Plenum Press, New York.
35. Wishart, D. S., Sykes, B. D., and Richards, F. M. (1991) *J. Mol. Biol. 222*, 311−333.
36. Lee, M. S., Palmer, A. G., III, and Wright, P. E. (1992) *J. Biomol. NMR 2*, 307−322.
37. Wishart, D. S., Bigam, C. G., Holm, A., Hodges, R. S., and Sykes, B. D. (1995) *J. Biol. NMR 5*, 67−81.
38. Kraulis, P. J. (1991) *J. Appl. Crystallogr. 24*, 946−950.
39. De Prat Gay, G., Johnson, C. M., and Fersht, A. R. (1994) *Protein Eng. 7*, 103−108.
40. Dao-Pin, S., Sauer, U., Nicholson, H., and Matthews, B. W. (1991) *Biochemistry 30*, 7142−7153.
41. Waldburger, C. D., Schildbach, J. F., and Sauer, R. T. (1995) *Nat. Struct. Biol. 2*, 122−128.
42. Riordan, J. F., McElvany, K. D., and Borders, C. L. (1977) *Science 195*, 884−886.
43. Borders, C. L., Broadwater, J. A., Bekeny, P. A., Salmon, J. E., Lee, S., Eldridge, M., and Pett, V. B. (1994) *Protein Sci. 3*, 541−548.
44. Mrabet, N. T., Van den Broeck, A., Van den Brande, I., Stanssens, P., Laroche, Y., Lambeir, A., Matthijssens, G., Jenkins, J., Chiadmi, M., van Tilbeurgh, H., Rey, F., Janin, J., Quax, W. J., Lasters, I., De Maeyer, M., and Wodak, S. J. (1992) *Biochemistry 31*, 2239−2253.
45. De Castiglione, R., Tam, J. P., Liu, W., Zhang, J. W., Galantino, M., Bertolero, F., and Vaghi, F. (1992) in *Peptides, Chemistry and Biology* (Smith, J. A., and Rivier, J. E., Eds.) pp 402−403, ESCOM, Leiden.
46. Richardson, J. S., and Richardson, D. C. (1988) *Science 240*, 1648−1652.
47. Scholtz, J. M., and Baldwin, R. L. (1995) in *Peptides: Synthesis, Structures, and Applications*, pp 171−192, Academic Press, San Diego, CA.
48. Hermans, J., Anderson, A. G., and Yun, R. H. (1992) *Biochemistry 31*, 5646−5653.
49. Galantino, M., De Castiglione, R., Tam, J. P., Liu, W., Zhang, J. W., Cristiani, C., and Vaghi, F. (1992) in *Peptides, Chemistry and Biology* (Smith, J. A., and Rivier, J. E., Eds.) pp 404−405, ESCOM, Leiden.
50. Tam, J. P., Dong, X., and Wu, C. R. (1992) in *Peptide Chemistry* (Yanaihara, N., Ed.), pp 24−26, ESCOM, Leiden.
51. Yanagisawa, M., Kurihara, H., Kimura, S., Tomobe, Y., Kobayashi, M., Mitsui, Y., Yazaki, Y., Goto, K., and Masaki T. (1988) *Nature 332*, 411−415.
52. Winther, J. R., and Sorensen, P. (1991) *Proc. Natl. Acad. Sci. U.S.A. 88*, 9330−9334.
53. Shinde, U., and Inouye, M. (1993) *Trends Biochem. Sci. 18*, 442−446.
54. Price-Carter, M., Gray, W. R., and Goldenberg, D. P. (1996) *Biochemistry 35*, 15537−15546.
55. Price-Carter, M., Gray, W. R., and Goldenberg, D. P. (1996) *Biochemistry 35*, 15547−15557.

BI9723764